J. COMBIN. MATH. COMBIN. COMPUT. 127b (2025) 7113--7139

Journal of Combinatorial Mathematics and Combinatorial Computing
www.combinatorialpress.com/jcmcc

Combinatorial Press

Quasi-periodic solutions of a non-autonomous KdV-mKdV equation with periodic unbounded conditions

Jumei Zhang[1,✉], Wenyan Cui[1], Honglun Wang[2]

[1] *College of Science, Shandong University of Aeronautics, Binzhou, Shandong, 256600, China*

[2] *Department of Information Engineering, Lubei Technician College, Binzhou, Shandong, 256600, China*

ABSTRACT

In this paper, the non-chiral boundary of the mixed kdv-mkdv equation is transformed into a chiral boundary by the construction of auxiliary functions, and a new linear difference format is constructed for the chiral boundary problem. Based on the traditional difference format, explicit and implicit differences are used alternately to construct a class of explicit-implicit (E-I) and implicit-explicit (I-E) alternating difference formats, and the unconditional stability of the numerical solutions is proved by taking advantage of the symmetric discrete numerical advantage of this class of alternating difference formats. The exact solution of the kdv-mkdv equation and its dynamical behavior are explored in the calculations using the semi-fixed separation of variables method combined with the phase diagram method for planar dynamical systems. Various types of exact solutions of the equations are obtained under special parametric conditions, and the existence problem of isolated wave solutions of the kdv-mkdv equations is analyzed in conjunction with the exact solutions of the equations. Numerical examples verify the accuracy and feasibility of the constructed differential format, indicating the existence of isolated wave solutions for the KdV-mKdV equation.

Keywords: kdV-mKdV equation, difference format, auxiliary function, non-chiral boundary, exact solution

1. Introduction

Initially, scholars proposed the nonlinear water wave equation used to study the water wave phenomenon, i.e., the KdV equation. Later, with the development of science, the KdV equation was gradually used to solve a series of scientific problems in optics, laser physics, chemistry, oceanography and so on [1-2]. As the research continued, it was found that there exists a Miura transformed equation between the KdV equations, i.e., the mKdV equations, where the solution of the mKdV equations can

✉ Corresponding author.
E-mail address: wdzjm02@163.com (J. Zhang).
Received 03 March 2024; Revised 20 April 2024; Accepted 10 November 2024; Published Online 16 April 2025.
DOI: 10.61091/jcmcc127b-388

be transformed into the solution of the KdV equations by the Miura transform, but not vice versa [3-5]. Nonlinear partial differential equations are an important branch of modern mathematics and have been widely used in the fields of mechanics, ecological and economic systems, and epidemiology [6-7]. The order of nonlinear partial differential equations can be integer or fractional [8]. With the birth of nonlinear partial differential equations of fractional order, exploring the exact solution of nonlinear partial differential equations of fractional order has become an important issue [9-10].

Many nonlinear phenomena occurring in nature can be described by nonlinear integrable equations, and nonlinear partial differential equations play an important role both in theoretical studies and in practical applications. However, for nonlinear partial differential equations, the solution problem is much more complicated than that of linear partial differential equations, and there is no unified solution method so far. To address the problem of solving the non chi-square KdV-mKdV equations, literature [11] analyzes the physical propagation properties and behaviors of isolated waves associated with the KdV-mKdV equations in the context of interactions, and mathematically investigates their algebraic and geometrical properties and plots them with different parameter values in order to form the solutions with kinks, singular periods and periodic behaviors. Literature [12] applied the fractal modification method to the KdV-mKdV combinatorial equation and used the chi-squared equilibrium method to construct the fractal Bäcklund transform, which can effectively derive the exact explicit solutions such as the periodic wave solutions of the trigonometric functions, and also solve the related graphical solutions with the help of software, which can provide a reference to the fractal theory of fractal partial differential equations. Literature [13] combines the radial basis function and the collocation method to solve the exact solution of the fractional order combinatorial KdV-mKdV equations, and calculates the error and stability of the numerical solution using the Mathematica program. Literature [14] utilizes the (G'/G) expansion and symbolic computation methods to construct rich traveling wave solutions of the KdV-mKdV equations, which can also incorporate constraints and have great potential for applications in physical sciences and engineering. Literature [15] proposes three exact solution methods for extracting exact soliton solutions of the KdV-mKdV equations, which, together with graphical simulation techniques, can be used to obtain more new solutions to the problem of solving the equations in question. However, the above studies are slightly insufficient in describing the proposed periodic behavior of nonlinear phenomena in nature, which are not approximated to periodic solutions with special properties, and the in-depth research work on the proposed periodic solutions of the non-chiral kdv-mkdv equations will be an important contribution to the development of mathematical physics.

In this paper, we propose a general form of the hybrid KdV-mKdV equation, which is simplified by a simple "scaling" transformation of the spatial variable x, the time variable t and the potential function $u(x,t)$. The N soliton solutions of the KdV-mKdV equation and their determinant forms are analyzed. Convert the non-chiral boundary problem of the KdV-mKdV equation into a chiral boundary by introducing auxiliary functions and constructing the difference format. The finite finite difference method is utilized to solve the KdV-mKdV equation. The exact solution of the KdV-mKdV equation is explored by means of an arithmetic example, respectively, and numerical simulation is applied to show the existence of an isolated wave solution for the KdV-mKdV equation. And numerical tests of the exact solution are applied to demonstrate the stability of the alternating difference method for the KdV-mKdV equation.

2. Description of the model and its exact solution

2.1. *KdV-mKdV equation*

The KdV and mKdV equations are two classical and important models in the theory of integrable systems [16-18]. A very interesting result is that the combined form of the KdV and mKdV equations is still an integrable nonlinear model because it has soliton solutions, integrable Hamiltonian systems, infinitely many conservation laws and Bäcklund transformations. For the hybrid KdV-mKdV equation, it was introduced at the same time as the discovery of the inverse scattering method before a series of research works by Wadati and Kodama. Later the hybrid KdV-mKdV equation was also known as the Gardner equation [19-20]. The hybrid KdV-mKdV equation in general form is:

$$u_t + \alpha u u_x + \beta u^2 u_x + \gamma u_{xxx} = 0 \tag{1}$$

Here $u = u(x,t)$ is the potential function, which describes the amplitude of the wave in question.

A simple "scaling" transformation of the spatial variable x, the time variable t and the potential function $u(x,t)$ is shown below:

$$x \to s_1 x, t \to s_2 t, u(x,t) \to s_3 u(x,t) \tag{2}$$

where there is when $\beta > 0$:

$$s_1 = \pm\alpha(6\gamma\beta)^{-\frac{1}{2}}, s_2 = \pm\alpha^3\gamma^{-\frac{1}{2}}(6\beta)^{-\frac{3}{2}}, s_3 = \frac{\alpha}{\beta} \tag{3}$$

Without loss of generality, the hybrid KdV-mKdV equation (1) can be written as:

$$u_t + 6uu_x + 6u^2 u_x + u_{xxx} = 0 \tag{4}$$

2.2. *Exact solution of the KdV-mKdV equation*

In order to obtain a solution to equation (1), assume:

$$u(x,t) = \sum_{i=0}^{m} a_l(t) T^i(\alpha(t)x + \beta(t)) \tag{5}$$

where $a_i(t), \alpha(t)$, $\alpha(t)$ and $\beta(t)$ are functions to be determined.

To determine the value of m, the chi-squared equilibrium method is utilized so that the nonlinear term is equal to the highest number of times of T in the highest order derivative term, i.e., $3m+1 = m+3$, yielding $m=1$. Substituting Eq. (5) into Eq. (1) using Maple software, and finally performing the transformation: $u(x,t) = u(\xi)$, $\xi = \alpha(t)x + \beta(t)$, yields the equation:

$$\begin{aligned} & a_1(t)\big[-\beta(t)\alpha'(t)T'(\xi) + \xi\alpha(t)T'(\xi) + \alpha(t)\beta'(t)T'(\xi)\big] \\ & + a_1(t)f(t)\alpha^2(t)T(\xi)T'(\xi) + a_0(t)f(t)\alpha^2(t)T'(\xi) \\ & + g(t)\alpha^2(t)a_1^2(t)T^2(\xi)T'(\xi) + 2a_0(t)a_1(t)g(t)\alpha^2(t)T(\xi)T'(\xi) \\ & + g(t)\alpha^2(t)a_0^2(t)T'(\xi) + h(t)\alpha^4(t)T'''(\xi) + l(t)\alpha^2(t)T'(\xi)\big] / \alpha(t) \end{aligned} \tag{6}$$

where $T(\xi)$ is satisfied:

$$\frac{dT}{d\xi} = \sqrt{p_0 + p_1 T + p_2 T^2 + p_3 T^3 + p_4 T^4} \tag{7}$$

$p_i (i = 0,1,\cdots,4)$ is a constant. In order to obtain an explicit expression for u, Eq. (7) is substituted into Eq. (5), and with the help of Maple software, a set of equations relating to $\alpha_i(t)$ $(i = 0,1)$, $\alpha(t)$, and $\beta(t)$ can be derived:

$$\alpha^2(t)\big(p_4 h(t)\alpha^2(t) + g(t)a_1^2(t)\big) = 0 \tag{8}$$

$$\alpha^2(t)\big(3p_4 h(t)\alpha^2(t) + 2a_0(t)a_1(t)g(t) + a_1(t)f(t)\big) = 0 \tag{9}$$

$$\begin{aligned}&\xi\alpha(t)-\beta(t)\alpha'(t)+\alpha(t)\beta'(t)+l(t)\alpha^2(t)\\&+a_0(t)f(t)\alpha^2(t)+g(t)a_0(t)\alpha^2(t)\end{aligned}\tag{10}$$

$$\begin{aligned}&p_2h(t)\alpha^2(t)=0\\&a_1(t)\neq 0\end{aligned}\tag{11}$$

Solving the above system of equations can be obtained with the help of Maple software:

$$\begin{aligned}&\alpha(t)=\alpha, a_0(t)=\frac{p_3\sqrt{-6p_4\alpha^2h(t)g(t)-2p_4f(t)}}{4p_4g(t)}\\&a_1^2(t)=-\frac{6p_4\alpha^2h(t)}{g(t)}\end{aligned}\tag{12}$$

$$\beta(t)=\frac{\alpha^3(3p_3^2-8p_2p_4)}{8p_4}\int h(t)dt-\alpha\int l(t)dt+\frac{\alpha}{4}\int\frac{f^2(t)}{g(t)}dt+C_1\tag{13}$$

where C_1 is an arbitrary constant. It can be concluded that the solution to the system of equations (1) is:

$$u(x,t)=\frac{p_3\sqrt{-6p_4\alpha^2h(t)g(t)-2p_4f(t)}}{4p_4g(t)}+\sqrt{-\frac{6p_4\alpha^2h(t)}{g(t)}}T(\xi)\tag{14}$$

Here, $\xi=\dfrac{(3\alpha^3p_3^2-8\alpha^3p_2p_4)\int h(t)dt+2\alpha p_4\int\frac{f^2(t)g(t)}{g(t)}dt-8\alpha p_4\int l(t)dt+8\alpha xp_4+8p_4C_1}{8p_4}$. An exact solution of equation (7) can be derived, and then many explicit exact solutions of equation (1) can be obtained from equation (8).

2.3. *N-soliton solutions of equations and their determinant forms*

2.3.1. Single soliton solutions. If it is still assumed that when $\varepsilon=1$, the perturbation expansion truncates to $w=1+w^{(1)}$ and $w^*=1+w^{(1)*}$, i.e., when $j=2,3,\cdots$, $w^{(j)}=0$. If we take the integral function $A(t)=0$ in Eq. (12) and have $w_{R_x}^{(1)}\neq 0$, we have for Eq. (13):

$$\frac{w_{R_x}^{(1)}w_{R_{xx}}^{(1)}-\left(w_{R_x}^{(1)}\right)^2}{\left(w_{R_x}^{(1)}\right)^2}=\left(\frac{w_{R_x}^{(1)}}{w_{R_x}^{(1)}}\right)_x=0\tag{15}$$

If $w_{R_{xx}}^{(1)}=0$, the solution is the same as the first rational solution. If $w_{R_{xx}}^{(1)}\neq 0$, it follows from equation (15):

$$\left(\frac{w_{R_x}^{(1)}}{w_{R_x}^{(1)}}\right)_x=\left(\ln w_{R_x}^{(1)}\right)_{xx}=0\tag{16}$$

This means that it is possible to take $w_{R_x}^{(1)}=e^{a_1(t)x+a_2(t)}$:

$$\begin{aligned}&w_R^{(1)}=\frac{1}{a_1(t)}e^{a_1(t)x+a_2(t)}+a_3(t)\\&w_1^{(1)}=w_{R_x}^{(1)}=e^{a_1(t)x+a_2(t)}\end{aligned}\tag{17}$$

where $a_1(t)$, $a_2(t)$, and $a_3(t)$ are all integral functions independent of x. Substituting Eq. (17) into (18) simplifies to obtain:

$$\left(a_1'(t)x+a_2'(t)+a_1^3(t)\right)e^{a_1(t)x+a_2(t)}=0 \tag{18}$$

It can be obtained that $a_1(t)=a_1$ can be any constant not equal to 0 $a_2'(t)=-a_1^3$, $a_2(t)=-a_1^3t+a_2$, a_2 are arbitrary constants. Notation $e^{\xi_1}=e^{a_1x-a_1^3+a_2}$ can be obtained:

$$\begin{aligned} w_R^{(1)} &= \frac{1}{a_1}e^{a_1x-a_1^3t+a_2}+a_3(t) \\ w_I^{(1)} &= e^{a_1x-a_1^3t+a_2} \end{aligned} \tag{19}$$

Substituting and simplifying Eq. (19) yields $a_3(t)=a_3$ as an arbitrary constant independent of t, x. Remember that $e^{a_1x-a_1^3t}=e^{\xi_1}$, $\frac{e^{\varepsilon_2}}{c_1}=\cos\theta_1$, $e^{c_2}=\sin\theta_1$, so there is:

$$w_1=1+w^{(1)}=1+e^{\xi_1+i\theta_1} \tag{20}$$

The first exponential function solution of the mixed KdV-mKdV equation, i.e., the single soliton solution is:

$$u=i\left(\ln\frac{w_1^*}{w_1}\right)_x=i\left(\ln\frac{1+e^{\xi_1-i\theta_1}}{1+e^{\xi_1+\theta_1}}\right)_x=\frac{a_1\left(a_1+a_3\right)}{1+\sqrt{1+a_1^2}\cosh\xi_1} \tag{21}$$

This completes the solution of the first exponential function with comprehension.

2.3.2. Two-soliton solutions. Assuming that $w^{(j)}=0$ when $j=3,4,\cdots$, the perturbative expansion truncates to $w=1+w^{(1)}+w^{(2)}$ and $w^*=1+w^{(1)^*}+w^{(2)^*}$ when $\varepsilon=1$. Since (16), (17) is a linear differential equation, it should also have a solution in additive form:

$$\begin{aligned} w_R^{(1)} &= e^{\xi_1}+e^{\xi_2} \\ w_{KI}^{(1)} = w_{R_x}^{(1)} &= a_1e^{\xi_1}+a_2e^{\xi_2} \end{aligned} \tag{22}$$

where $\xi_1=a_1x+b_1t+c_1$, and $\xi_2=a_2x+b_2t+c_2$. Substituting Eq. (22) into (17) simplifies to obtain:

$$w_{I_t}^{(1)}+w_{I_{xxx}}^{(1)}=\left(a_1b_1+a_1^4\right)e^{\xi_1}+\left(a_2b_2+b_2^4\right)e^{\xi_2}=0 \tag{23}$$

That is, $b_1=-a_1^3$, and $b_2=-a_2^3$, which is obtained by substituting Eq. (22) into (16) to simplify:

$$w_{I_x}^{(2)}-w_{R_{xx}}^{(2)}=a_1a_2\left(a_1-a_2\right)^2e^{\xi_1+\xi_2} \tag{24}$$

Substituting equation (22) into (17) simplifies to:

$$w_{I_t}^{(2)}+w_{I_{xxx}}^{(2)}=3a_1a_2\left(a_1-a_2\right)^2e^{\xi_1+\xi_2} \tag{25}$$

Therefore it can be assumed:

$$w_I^{(2)}=k_1e^{\xi_1+\xi_2} \tag{26}$$

Then there is:

$$w_{I_t}^{(2)}+w_{I_{xxx}}^{(2)}=3a_1a_2k_1\left(a_1+a_2\right)^2e^{\xi_1-\xi_2} \tag{27}$$

And so it can be sought:

$$k_1 = \frac{(a_1 - a_2)^2}{(a_1 + a_2)^2} \tag{28}$$

That is to say:

$$w_I^{(2)} = \frac{(a_1 - a_2)^2}{(a_1 + a_2)^2} e^{\xi_1 + \xi_2} \tag{29}$$

Substituting equation (29) into (25) gives:

$$w_{R_{xx}}^{(2)} = (1 - a_1 b_1)(a_1 - b_1)^2 e^{\xi_1 + \xi_2} \tag{30}$$

Integrating x twice and simply taking the constant of integration to be 0 yields:

$$w_R^{(2)} = \frac{(1 - a_1 a_2)(a_1 - a_2)^2}{a_1 + a_2^2} e^{\xi_1 + \xi_2} \tag{31}$$

Substituting Eqs. (22), (30), and (31) into Eqs. (16) and (17) simplifies the right-hand side to 0, i.e., taking $w^{(j)} = 0, j = 3, 4, \cdots$ so that the truncated form of the series $w_2 = 1 + w^{(1)} + w^{(2)}$. Remember that $e^{c_1} = \cos\theta_1$, $a_1 e^{c_1} = \sin\theta_1$, $\frac{(a_1 - a_2)^2}{(a_1 + a_2)^2} = e^{A_{12}}$, $e^{c_2} = \cos\theta_2$, $a_2 e^{c_2} = \sin\theta_2$. Thus the second soliton solution of the hybrid Kdv-mKdV equation is written:

$$u = i\left(\ln \frac{1 + e^{\xi_1 - i\theta_1} + e^{\xi_2 - i\theta_2} + e^{\xi_1 + \xi_2 - i(\theta_1 + \theta_2) + A_{12}}}{1 + e^{\xi_1 + i\theta_1} + e^{\xi_2 + i\theta_1} + e^{\xi_1 + \xi_2 + i(\theta_1 + \theta_2) + A_{12}}}\right)_x \tag{32}$$

2.3.3. N soliton solutions. Typically, if taken:

$$w_R^{(1)} = e^{\xi_1} + e^{\xi_2} + \cdots + e^{\xi_N}, w_I^{(1)} = w_{R_x}^{(1)} = a_1 e^{\xi_1} + a_2 e^{\xi_2} + \cdots + a_j e^{\xi_N} \tag{33}$$

where $\xi_j = a_j x + b_j^3 t$, $b_j = -a_j^3$, $\tan\theta_j = a_j$, $j = 1, 2, \cdots, N$. The truncated expression for the level at $\varepsilon = 1$ is then obtained by induction:

$$w_N(t, x) = \sum_{\mu=0,1} e^{\sum_{j=1}^{N} \mu_j(\xi_j + i\theta_j) + \sum_{1 \le j < l}^{N} \mu_j \mu_l A_{jl}} \tag{34}$$

The exponential part of the sum of μ denotes the sum of all terms when $\mu_j\,(j = 1, 2, \cdots, N)$ takes 0 or 1, where $e^{A_{jl}} = \left(\frac{k_j - k_l}{k_j + k_l}\right)^2$. Then the N th exponential function solution of the hybrid Kdv-mKdV equation is:

$$u = i\left[\ln \frac{\sum_{\mu=0,1} e^{\sum_{j=1}^{N} \mu_j(\xi_j - i\theta_j) + \sum_{1 \le j \le l}^{N} \mu_j \mu_l A_{jl}}}{\sum_{\mu=0,1} e^{\sum_{j=1}^{N} \mu_j(\xi_j + i\theta_j) + \sum_{1 \le j \le l}^{N} \mu_j \mu_l A_{jl}}}\right]_x \tag{35}$$

For the above result, consider the determinantal representation of its exponential function solution.

3. Differential calculation of equations

The study of nonlinear wave phenomena is an important topic in nonlinear research, and the nonchiral boundary problem has been a difficult problem in the study of nonlinear fluctuation problems. There are many methods for the treatment of non-chiral boundaries, and the finite difference method can also be applied to the treatment of non-chiral boundary conditions.

In this paper, we consider applying the finite difference method to the non-chiral boundary kdv-mkdv equations for solving the kdv-mkdv equations.

3.1. Construction of Differential Formats

In order to solve the non-chiral boundary problem for the KdV-mKdV equation, a new function is introduced to convert the non-chiral boundary into a chiral boundary.

An auxiliary function is introduced:

$$u(x,t)=v(x,t)+\theta_1(t)x^3+\theta_2(t)x^2+\theta_3(t)x+\theta_4(t) \tag{36}$$

where $\theta_1(t),\theta_2(t),\theta_3(t),\theta_4(t)$ are four unknown functions to be determined and satisfy $v(x,t)=0$. The following system of equations for $\theta_1(t),\theta_2(t),\theta_3(t),\theta_4(t)$ can be obtained from equations (1)-(5):

$$\begin{cases}\theta_1(t)x_t^3+\theta_2(t)x_1^2+\theta_3(t)x_t+\theta_4(t)=a_1(t)\\ \theta_1(t)x_r^3+\theta_2(t)x_r^2+\theta_3(t)x_r+\theta_4(t)=a_2(t)\\ 6\theta_1(t)x_t+2\theta_2(t)=b_1(t)\\ 6\theta_1(t)x_r+2\theta_2(t)=b_2(t)\end{cases} \tag{37}$$

The solution to the system of equations can be found as:

$$\begin{cases}\theta_1(t)=\dfrac{b_1(t)-b_2(t)}{6L}\\ \theta_2(t)=\dfrac{b_2(t)x_l-b_1(t)x_r}{2L}\\ \theta_3(t)=\dfrac{a_1(t)-a_2(t)}{L}-\dfrac{b_1(t)+2b_2(t)}{6L}x_l^2\\ \qquad+\dfrac{2b_1(t)+b_2(t)}{6L}x_r^2+\dfrac{b_1(t)-b_2(t)}{3L}x_ix_r\\ \theta_4(t)=\dfrac{a_2(t)x_l-a_1(t)x_r}{L}-\dfrac{2b_1(t)+b_2(t)}{6L}x_lx_r^2\\ \qquad+\dfrac{b_1(t)+2b_2(t)}{6L}x_l^2x_r\end{cases} \tag{38}$$

where $L=x_r-x_l$.

Substituting Eq. (37) into Eqs. (1)-(4), we have:

$$\begin{aligned}&v_t+v_{xxxxt}+v_x+\lambda^{kdv}v_{xxx}+w_x+g_2(x,t)v_x\\&=f(x,t)\left(x\in[x_t,x_r],t\in[x_t,x_r]\right)\end{aligned} \tag{39}$$

$$\begin{aligned}v(x,0)=u_0(x)-\theta_1(0)x^3-\theta_2(0)x^2\\ -\theta_3(0)x-\theta_4(0)\left(x\in[x_i,x_r]\right)\end{aligned} \tag{40}$$

$$\begin{aligned}&v(x_l,t)=0,v(x_r,t)=0,v_{xx}(x_l,t)=0\\&v_{xx}(x_r,t)=0(t\in[0,T])\end{aligned} \tag{41}$$

Among them:

$$
\begin{aligned}
&g_1(x,t)=3\theta_1(t)x^2+2\theta_2(t)x+\theta_3(t)\\
&g_2(x,t)=\theta_1(t)x^3+\theta_2(t)x^2+\theta_3(t)x+\theta_4(t)\\
&g_3(x,t)=\theta_1'(t)x^3+\theta_2'(t)x^2+\theta_3'(t)x+\theta_4'(t)\\
&f(x,t)=-g_3(x,t)-g_1(x,t)-g_2(x,t)\cdot g_1(x,t)-6\lambda^{kdv}\theta_1(t)
\end{aligned} \tag{42}
$$

The following dissects the region $[x_l,x_r]\times[0,T]$ by taking positive integers J and N, such that the spatial step $h=\frac{x_r-x_l}{J}$ and the temporal step $\tau=\frac{L}{N}$, and noting $x_j=x_l+jh\left(0\le j\le J\right)$, $t^n=n\tau\left(0\le n\le N\right)$, $v_j^n=v(x_j,t^n)$, define $Z_h^0=\left\{v=(v_j)\,|\,v_{-1}=v_0=v_J=v_{J+1}=0\left(-1\le j\le J+1\right)\right\}$, and for any two grid functions $u^n,v^n\in Z_h^0$, define the inner product and the paradigm in the following notation:

$$\left(v_j^n\right)_x=\frac{v_{j+1}^n-v_j^n}{h},\left(v_j^n\right)_{\bar{x}}=\frac{v_j^n-v_{j-1}^n}{h} \tag{43}$$

$$\left(v_j^n\right)_{\hat{x}}=\frac{v_{j+1}^n-v_{j-1}^n}{2h},\bar{v}_j^n=\frac{v_j^{n+1}+v_j^{n-1}}{2} \tag{44}$$

$$\left(v_j^n\right)_t=\frac{v_j^{n+1}-v_j^n}{\tau},\left(v_j^n\right)_{\hat{t}}=\frac{v_j^{n+1}-v_j^{n-1}}{2\tau} \tag{45}$$

$$\bar{t}=\frac{t^{n+1}+t^{n-1}}{2} \tag{46}$$

$$\left\langle u^n,v^n\right\rangle=h\sum_{j=1}^{j-1}u_j^nv_j^n,\left\|v^n\right\|^2=\left\langle v^n,v^n\right\rangle \tag{47}$$

$$\left\|v^n\right\|_\infty=\max_{1\le j\le J-1}\left|v_j^n\right| \tag{48}$$

Consider the following three-level linear finite difference format for problems (39)-(41):

$$
\begin{aligned}
&\left(v_j^n\right)_{\hat{t}}+\left(v_j^n\right)_{x\bar{x}x\bar{x}\hat{t}}+\left(\bar{v}_j^n\right)_{\hat{x}}+\lambda^{kdv}\left(\bar{v}_j^n\right)_{x\bar{x}\hat{x}}+\varphi\left(v_j^n,\bar{v}_j^n\right)\\
&+\left\{g_2\left(x_j,\bar{t}^n\right)\bar{v}_j^n\right\}_{\hat{x}}=f\left(x_j,\bar{t}^n\right),\left(1\le j\le J-1,2\le n\le N\right)
\end{aligned} \tag{49}
$$

$$v_j^0=u_0\left(x_j\right)-\theta_1(0)x_j^3-\theta_2(0)x_j^2-\theta_3(0)x_j-\theta_4(0)\left(1\le j\le J-1\right) \tag{50}$$

$$v_0^n=0,v_J^n=0,\left(v_0^n\right)_{x\bar{x}}=0,\left(v_J^n\right)_{x\bar{x}}=0 \tag{51}$$

where $\varphi\left(v_j^n,\bar{v}_j^n\right)=\frac{1}{3}\left[v_j^n\left(\bar{v}_j^n\right)_{\hat{x}}+\left(v_j^n\bar{v}_j^n\right)_{\hat{x}}\right]$. Since the difference format is a three-layer format, a two-layer format is given below to solve for v^1:

$$
\begin{aligned}
&\left(v_j^0\right)_t+\left(v_j^0\right)_{x\bar{x}x\bar{x}t}+\left(v_j^{\frac{1}{2}}\right)_{\hat{x}}+\lambda^{kdv}\left(v_j^{\frac{1}{2}}\right)_{x\bar{x}\hat{x}}+\varphi\left(v_j^0,v_j^{\frac{1}{2}}\right)+\left\{g_2\left(x_j,t^{\frac{1}{2}}\right)v_j^{\frac{1}{2}}\right\}_{\hat{x}}\\
&=f\left(x_j,t^{\frac{1}{2}}\right)\left(1\le j\le J-1,2\le n\le N\right)
\end{aligned} \tag{52}
$$

Of these, $v_j^{\frac{1}{2}}=\dfrac{v_j^0+v_j^1}{2}$, $t^{\frac{1}{2}}=\dfrac{t^0+t^1}{2}$.

3.2. Stability of Differential Formats

Theorem 1: Differential formats are unconditionally stable.

Proof: consider only the chi-square case, i.e:

$$\begin{aligned}&\left(v_j^n\right)_i+\left\{\alpha+\beta\left[\theta_1\left(\bar{i}^n\right)x_j^2+\theta_2\left(\bar{i}^n\right)x_j+\theta_3\left(\bar{i}^n\right)\right]\right\}\\&\left(\bar{v}_j^n\right)_{\hat{x}}+\beta\varphi\left(v_j^n,\bar{v}_j^n\right)+\gamma\left(\bar{v}_j^n\right)_{xx\hat{x}}=0\end{aligned}\tag{53}$$

Using vonNeumann stability analysis, let $v_j^n=\varepsilon^n e^{ij\theta}$, where $i^2=-1,\theta$ is the wave number, have:

$$(v_j^n)_t=\frac{1}{2\tau}\varepsilon^n e^{ij\theta}(\varepsilon-\varepsilon^{-1})\tag{54}$$

$$\begin{aligned}&\left\{\alpha+\beta\left[\theta_1(t^n)x_j^2+\theta_2(t^n)x_j+\theta_3(t^n)\right]\right\}(v_j^n)_x\\&=\frac{1}{2h}\left\{\alpha+\beta\left[\theta_1(t^n)x_j^2+\theta_2(t^n)x_j+\theta_3(t^n)\right]\right\}i\sin\theta\varepsilon^n e^{ij\theta}(\varepsilon+\varepsilon^{-1})\end{aligned}\tag{55}$$

$$\begin{aligned}\beta\varphi(v_j^n,\bar{v}_j^n)&=\frac{\beta}{3}\left\{v_j^n(\bar{v}_j^n)_x+[v_x^n(\bar{v}_j^n)]\right\}\\&=\frac{\beta}{6h}v_j^n i\sin\theta\varepsilon^n e^{ij\theta}(\varepsilon+\varepsilon^{-1})+\frac{\beta}{6h}v_j^n i\sin\theta\varepsilon^n e^{ij\theta}(\varepsilon+\varepsilon^{-1})\\&=\frac{\beta}{3h}v_j^n i\sin\theta\varepsilon^n e^{ij\theta}(\varepsilon+\varepsilon^{-1})\end{aligned}\tag{56}$$

$$\gamma(\bar{v}_j^n)_{xx\hat{x}}=\frac{\gamma}{2h^3}i(\sin2\theta-2\sin\theta)\varepsilon^n e^{ij\theta}(\varepsilon+\varepsilon^{-1})\tag{57}$$

Substituting (54)~(57) into (53) yields $\varepsilon^2=\dfrac{1-iB}{1+iB}$, where:

$$\begin{aligned}B=\frac{\tau}{h}&\left\{\left[\alpha+\beta\left(\theta_1(t^n)x_j^2+\theta_2(t^n)x_j+\theta_3(t^n)\right)\right]\sin\theta\right.\\&\left.+\frac{\gamma}{h^2}(\sin2\theta-2\sin\theta)+\frac{2\beta}{3}v_j^n\sin\theta\right\}\end{aligned}\tag{58}$$

This leads to $|\varepsilon|=1$, so the differential format is unconditionally stable.

3.3. Explicit and implicit alternating difference methods for the KdV equation

Equation (1) degenerates into the KdV equation when $\alpha\neq0$, $\beta=0$, $\varepsilon=0$, $\gamma\neq0$, i.e:

$$\partial_t u+\alpha u\partial_x u+\gamma\partial_{xxx}u=0\tag{59}$$

The KdV equation is a partial differential equation for unidirectional motion shallow water waves discovered by the Dutch mathematicians Kottweg and de Vries. The dispersion coefficient in the equation satisfies $\gamma>0$, and the equation is used to describe many phenomena in physics, such as magnetohydrodynamic waves in cold ionized bodies and nonlinear waves in liquid-bubble mixtures. The E-I difference format of a class of KdV equations is given below as follows:

$$\begin{cases} \dfrac{U_j^{2n+1}-U_j^{2n}}{k}+\dfrac{\alpha a_j^{2n}k}{2h}(U_{j+1}^{2n}-U_{j-1}^{2n}) \\ +\dfrac{\gamma k}{2h^3}(-U_{j-2}^{2n}+4U_j^{2n}-4U_{j+1}^{2n}+U_{j+2}^{2n})=0 \\ \dfrac{U_j^{2n+2}-U_j^{2n+1}}{k}+\dfrac{\alpha a_j^{2n}k}{2h}(U_{j+1}^{2n+1}-U_{j-1}^{2n+1}) \\ +\dfrac{\gamma k}{2h^3}(-U_{j-2}^{2n+1}+4U_j^{2n+1}-4U_{j+1}^{2n+1}+U_{j+2}^{2n+1})=0 \end{cases} \tag{60}$$

into matrix form:

$$\begin{cases} U^{2n+1}=(I-G^{2n})U^{2n}+g^{2n} \\ (I+G^{2n})U^{2n+2}=U^{2n+1}+g^{2n+2} \end{cases} \tag{61}$$

Among them:

$$G^n=\begin{pmatrix} 4r & c_j^n-4r & r & & & & \\ -c_j^n & 4r & c_j^n-4r & r & & & \\ -r & -c_j^n & 4r & c_j^n-4r & r & & \\ & \ddots & \ddots & \ddots & \ddots & \ddots & \\ & & -r & -c_j^n & 4r & c_j^n-4r & r \\ & & & -r & -c_j^n & 4r & c_j^n-4r \\ & & & & -r & -c_j^n & 4r \end{pmatrix}_{(M-3)\times(M-3)} \tag{62}$$

I is a unit matrix of order $(M-3)\times(M-3)$. $U^n=[U_2^n,U_3^n,\cdots,U_{M-2}^n]^T$, $a_j^{2n}=\dfrac{U_{j-1}^{2n}+2U_j^{2n}+U_{j+1}^{2n}}{4}$, $c_j^n=\dfrac{\alpha a_j^{2n}k}{2h}$, $r=\dfrac{\gamma k}{2h^3}$, U^n and g^n are both $(M-3)$-dimensional vectors, $g^n=\left[rU_0^n+c_j^nU_1^n,rU_1^n,\cdots,-rU_{M-1}^n,-(c_j^n-4r)U_{M-1}^n-rU_M^n\right]^T$.

The I-E difference format of the KdV equation is as follows:

$$\begin{cases} \dfrac{U_j^{2n+1}-U_j^{2n}}{k}+\dfrac{\alpha a_j^{2n}k}{2h}(U_{j+1}^{2n+1}-U_{j-1}^{2n+1}) \\ +\dfrac{\gamma k}{2h^3}(-U_{j-2}^{2n+1}+4U_j^{2n+1}-4U_{j+1}^{2n+1}+U_{j+2}^{2n+1})=0 \\ \dfrac{U_j^{2n+2}-U_j^{2n+1}}{k}+\dfrac{\alpha a_j^{2n}k}{2h}(U_{j+1}^{2n+1}-U_{j-1}^{2n+1}) \\ +\dfrac{\gamma k}{2h^3}(-U_{j-2}^{2n+1}+4U_j^{2n+1}-4U_{j+1}^{2n+1}+U_{j+2}^{2n+1})=0 \end{cases} \tag{63}$$

into matrix form:

$$\begin{cases} (I+G^{2n})U^{2n+1}=U^{2n}+g^{2n+1} \\ U^{2n+2}=(I-G^{2n})U^{2n+1}+g^{2n+1} \end{cases} \tag{64}$$

where G^n, g^n are defined in the same matrix form (61).

Similar to the numerical analysis of the E-I difference format of the combined KdV-Burgers equation with variable coefficients, the following theorem can be derived identically.

Theorem 2: The E-I difference format (60) and the I-E difference format (62) of the KdV equation are uniquely solvable, linearly absolutely stable and linearly convergent, and satisfy:

$$\left\| u_j^n - U_j^n \right\| \le C(k^2 + h^2), n = 1, 2, \cdots N \tag{65}$$

where C is a positive constant.

3.4. Explicit and implicit alternating difference methods for the KdV-mKdV equation

When $\alpha \neq 0$, $\beta \neq 0$, $\varepsilon = 0$, $\gamma \neq 0$, the equations degenerate into the well-known KdV-mKdV equations, viz:

$$\partial_t u + \alpha u \partial_x u + \beta u^2 \partial_x u + \gamma \partial_{xxx} u = 0 \tag{66}$$

The $KdV - mKdV$ equation is a hybrid version of the KdV equation and the $mKdV$ equation, which is a nonlinear development equation found earlier and representative. It has very important applications in the fields of mathematics, physics and engineering, etc. The dispersion coefficient in the equation satisfies $\gamma > 0$. The E-I difference format of the KdV-mKdV equation is given below as follows:

$$\begin{cases} \dfrac{U_j^{2n+1} - U_j^{2n}}{k} + \dfrac{\alpha a_j^{2n} k}{2h}(U_{j+1}^{2n} - U_{j-1}^{2n}) + \dfrac{\beta (a_j^{2n})^2 k}{2h}(U_{j+1}^{2n} - U_{j-1}^{2n}) \\ + \dfrac{\gamma k}{2h^3}(-U_{j-2}^{2n} + 4U_j^{2n} - 4U_{j+1}^{2n} + U_{j+2}^{2n}) = 0 \\ \dfrac{U_j^{2n+2} - U_j^{2n+1}}{k} + \dfrac{\alpha a_j^{2n} k}{2h}(U_{j+1}^{2n+1} - U_{j-1}^{2n+1}) + \dfrac{\beta (a_j^{2n})^2 k}{2h}(U_{j+1}^{2n+1} - U_{j-1}^{2n+1}) \\ + \dfrac{\gamma k}{2h^3}(-U_{j-2}^{2n+1} + 4U_j^{2n+1} - 4U_{j+1}^{2n+1} + U_{j+2}^{2n+1}) = 0 \end{cases} \tag{67}$$

into matrix form:

$$\begin{cases} U^{2n+1} = (I - G^{2n})U^{2n} + g^{2n} \\ (I + G^{2n})U^{2n+2} = U^{2n+1} + g^{2n+2} \end{cases} \tag{68}$$

I is a unit matrix of order $(M-3)\times(M-3)$. $U^n = [U_2^n, U_3^n, \cdots, U_{M-2}^n]^T$, $a_j^{2n} = \dfrac{U_{j-1}^{2n} + 2U_j^{2n} + U_{j+1}^{2n}}{4}$, $c_j^n = \dfrac{\alpha a_j^{2n} k}{2h}$, $d_j^n = \dfrac{\beta (a_j^{2n})^2 k}{2h}$, $r = \dfrac{\gamma k}{2h^3}$. Both U^n and g^n are $(M-3)$ dimensional vectors.

and $g^n = \left[rU_0^n - (c_j^n + d_j^n)U_1^n, rU_1^n, \cdots, -rU_{M-1}^n, -(c_j^n + d_j^n - 4r)U_{M-1}^n - rU_M^n \right]^T$.

The I-E difference format for the KdV-mKdV equation is as follows:

$$\begin{cases} \dfrac{U_j^{2n+1} - U_j^{2n}}{k} + \dfrac{\alpha a_j^{2n} k}{2h}(U_{j+1}^{2n+1} - U_{j-1}^{2n+1}) + \dfrac{\beta (a_j^{2n})^2 k}{2h}(U_{j+1}^{2n+1} - U_{j-1}^{2n+1}) \\ + \dfrac{\gamma k}{2h^3}(-U_{j-2}^{2n+1} + 4U_j^{2n+1} - 4U_{j+1}^{2n+1} + U_{j+2}^{2n+1}) = 0 \\ \dfrac{U_j^{2n+2} - U_j^{2n+1}}{k} + \dfrac{\alpha a_j^{2n} k}{2h}(U_{j+1}^{2n+1} - U_{j-1}^{2n+1}) + \dfrac{\beta (a_j^{2n})^2 k}{2h}(U_{j+1}^{2n+1} - U_{j-1}^{2n+1}) \\ + \dfrac{\gamma k}{2h^3}(-U_{j-2}^{2n+1} + 4U_j^{2n+1} - 4U_{j+1}^{2n+1} + U_{j+2}^{2n+1}) = 0 \end{cases} \tag{69}$$

into matrix form:

$$\begin{cases}(I+G^{2n})U^{2n+1}=U^{2n}+g^{2n+1} \\ U^{2n+2}=(I-G^{2n})U^{2n+1}+g^{2n+1}\end{cases} \tag{70}$$

where G^n, g^n are defined in the same matrix form (68).

Assuming that the coefficients $a_j^n=a$ in equation G^n are constants and that $G^n=G$, the following calculations are performed in this case. Since the dispersion coefficient $\gamma>0$, the matrix $G+G^T$ is obtained to be non-negative definite.

From Theorem 2, it follows that $(I+G)^{-1}$ exists, and thus there are unique solutions for the E-I difference format (67) and the I-E difference format (69). The proof of the linear absolute stability and linear convergence of the E-I difference format of the KdV-Burgers equation for combinations of coefficients of the same variable is given by the following theorem.

Theorem 3: The E-I difference format (67) and the I-E difference format (69) of the KdV-mKdV equation are uniquely solvable, linearly absolutely stable, and linearly convergent and satisfy:

$$\left\|u_j^n-U_j^n\right\|\le C(k^2+h^2),n=1,2,\cdots N \tag{71}$$

where C is a positive constant.

4. Numerical examples

4.1. Example 1

The exact solutions of the KdV-mKdV equation are explored here in the following three categories.

1) $g=0$

When $g=0$, $\rho<0$, $O(0,0)$ is a higher-order singularity because $J_O(0,0)=0$ and the equilibrium point index is not zero.

When $g=0$, the phase diagram of the planar dynamical system is shown in Fig. 1, which is a phase diagram of the system drawn using Maple software. In order to distinguish the types of orbits in the graph, black lines are used to indicate orbits with h values equal to zero, blue lines are used to indicate orbits with h values greater than zero, green colors are used to indicate orbits with h values less than zero, and rosy red lines are used to mark singularities.

Corresponding to the rectilinear black orbits in Phase Figure 1(a), substituting $h=h_O=0$ into the planar dynamical system yields:

$$y=\pm\frac{v}{\sqrt{-\rho}} \tag{72}$$

Substituting Eq. (72) into $\frac{dv}{dx}=y$ for the planar dynamical system solves:

$$v_1=C_1e^{\frac{1}{\sqrt{-\rho}}x},v_2=C_2e^{-\frac{1}{\sqrt{-\rho}}x} \tag{73}$$

where C_1 and C_2 are constants. Substituting v_1 and v_2 back into the first equation in the system of equations (8) in equation (73), respectively, yields:

$$\frac{C_1(\rho-\beta)}{\rho\sqrt{-\rho}}e^{\frac{x}{\sqrt{-\rho}}}=0,\frac{C_2(\rho-\beta)}{\rho\sqrt{-\rho}}e^{-\frac{x}{\sqrt{-\rho}}}=0 \tag{74}$$

A common parametric condition is solved by equation (74):

$$\beta=\rho \tag{75}$$

This is a condition where dissipation is in equilibrium with diffusion. Thus, when $\beta=\rho$, substituting v_1 and v_2 into equation (3) yields two exact solutions of equation (2):

$$u_1(x,t) = C_1 e^{\frac{1}{\sqrt{-\rho}}x} E_\alpha\left(\lambda t^\alpha\right) \tag{76}$$

$$u_2(x,t) = C_2 e^{-\frac{1}{\sqrt{-\rho}}x} E_\alpha\left(\lambda t^\alpha\right) \tag{77}$$

If the initial edge value condition is given, one can obtain a special solution for $u(x,t)$.
For example, if u_1 and u_2 satisfy the initial edge value condition:

$$u_1(0,t) = E_\alpha(-2t^\alpha), u_1(x,0) = e^{\frac{1}{\sqrt{-\rho}}x} \tag{78}$$

$$u_2(0,t) = E_\alpha(-2t^\alpha), u_2(x,0) = e^{-\frac{1}{\sqrt{-\rho}}x} \tag{79}$$

Then the corresponding special solution is:

$$u_1(x,t) = e^{\frac{1}{\sqrt{-\rho}}x} E_\alpha\left(-2t^\alpha\right) \tag{80}$$

$$u_2(x,t) = e^{-\frac{1}{\sqrt{-\rho}}x} E_\alpha\left(-2t^\alpha\right) \tag{81}$$

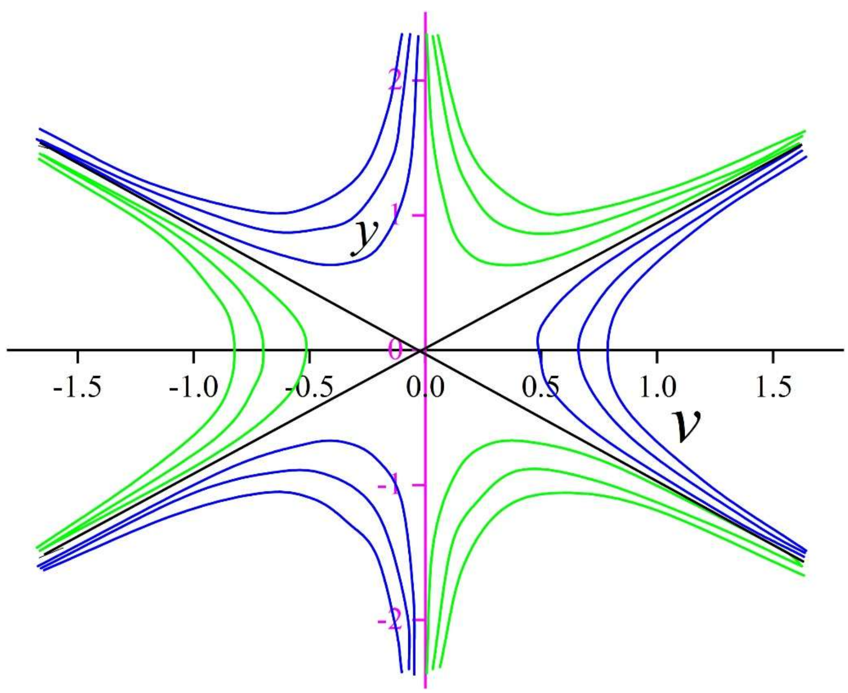

(a) $g = 0, \rho < 0$

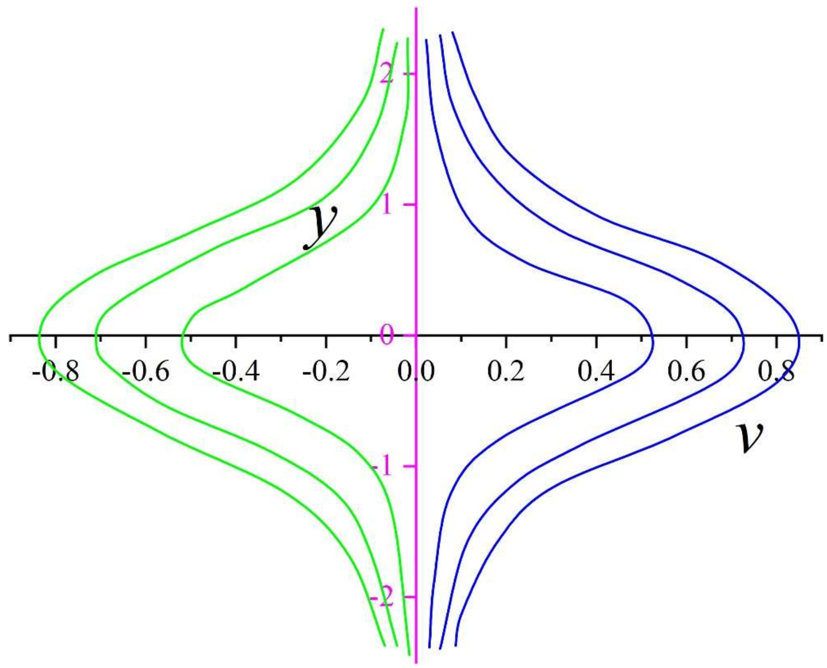

(b) $g=0, \rho>0$

Fig. 1. The plane power system at g=0

2) $g>0$

When $g>0$ and $\rho>0$, $J_{A_{1,2}}(\pm\sqrt{\frac{g}{3}},0)=4\rho g>0$ and $\mathrm{trace}M(v,y)\equiv 0$. Then $A_{1,2}\left(\pm\sqrt{\frac{g}{3}},0\right)$ are centered.

Since $J_{B_{1,2}}(0,\pm\sqrt{\frac{g}{\rho}})=-4\rho g<0$, then $B_{1,2}\left(0,\pm\sqrt{\frac{g}{\rho}}\right)$ are saddle points. When $g>0$ and $\rho<0$, there is $J_{A_{1,2}}(\pm\sqrt{\frac{g}{3}},0)=4\rho g<0$. Then $A_{1,2}\left(\pm\sqrt{\frac{g}{3}},0\right)$ are all saddle points, while $B_{1,2}\left(0,\pm\sqrt{\frac{g}{\rho}}\right)$ do not exist.

Based on the above information about the equilibrium point, the phase diagram of the planar dynamical system under the parametric condition $g>0$ is drawn using Maple software. The phase diagram of the planar dynamical system for $g>0$ is shown in Fig. 2.

Corresponds to the black orbit in Fig. 2(a), obtained by substituting $h=h_{B_{1,2}}=0$:

$$y=\pm\sqrt{\frac{g}{\rho}-\frac{v^2}{\rho}} \tag{82}$$

Substituting Eq. (82) into $\frac{dv}{dx}=y$ for the planar dynamical system yields:

$$\frac{dv}{\pm\sqrt{\frac{g}{\rho}-\frac{v^2}{\rho}}}=dx \tag{83}$$

When $\rho>0$, integrating both sides of (83) simultaneously yields:

$$\begin{aligned} v_3 &= \sqrt{g}\sin\left(\frac{x}{\sqrt{\rho}}+C_3\right) \\ v_4 &= -\sqrt{g}\sin\left(\frac{x}{\sqrt{\rho}}+C_4\right) \end{aligned} \tag{84}$$

When $\rho < 0$, then integrate both sides of (84) simultaneously to get:

$$\begin{aligned} v_5 &= \sqrt{g}\cosh\left(\frac{x}{\sqrt{-\rho}}+C_5\right) \\ v_6 &= -\sqrt{g}\cosh\left(\frac{x}{\sqrt{-\rho}}+C_6\right) \end{aligned} \tag{85}$$

where C_3, C_4, C_5 and C_6 are arbitrary constants. Substituting v_3, v_4, v_5 and v_6 into the first equation of the system of equations (8), respectively, similar to the computational procedure of the previous (75) and (76), the parametric condition $\beta=\rho$ is also obtained. This is the compatibility condition for the same solution of the two equations in the system of equations (8).

Thus, when $\beta=\rho$, the four exact solutions of equation (2) are obtained by substituting v_3, v_4, v_5, and v_6 into equation (3), respectively. Namely:

$$u_3(x,t)=\sqrt{g}\sin\left(\frac{x}{\sqrt{\rho}}+C_3\right)E_\alpha\left(\lambda t^\alpha\right) \tag{86}$$

$$u_4(x,t)=-\sqrt{g}\sin\left(\frac{x}{\sqrt{\rho}}+C_4\right)E_\alpha\left(\lambda t^\alpha\right) \tag{87}$$

$$u_5(x,t)=\sqrt{g}\cosh\left(\frac{x}{\sqrt{-\rho}}+C_5\right)E_\alpha\left(\lambda t^\alpha\right) \tag{88}$$

$$u_6(x,t)=-\sqrt{g}\cosh\left(\frac{x}{\sqrt{-\rho}}+C_6\right)E_\alpha\left(\lambda t^\alpha\right) \tag{89}$$

Similarly, special solutions of the original equations can be obtained under appropriate conditions for the values of the initial margins. In particular, take:

$$u_3(x,t)=\sqrt{2}\sin\left(\frac{x}{\sqrt{\rho}}\right)E_\alpha\left(-2t^\alpha\right) \tag{90}$$

$$u_5(x,t)=\sqrt{2}\cosh\left(\frac{x}{\sqrt{-\rho}}\right)E_\alpha\left(-2t^\alpha\right) \tag{91}$$

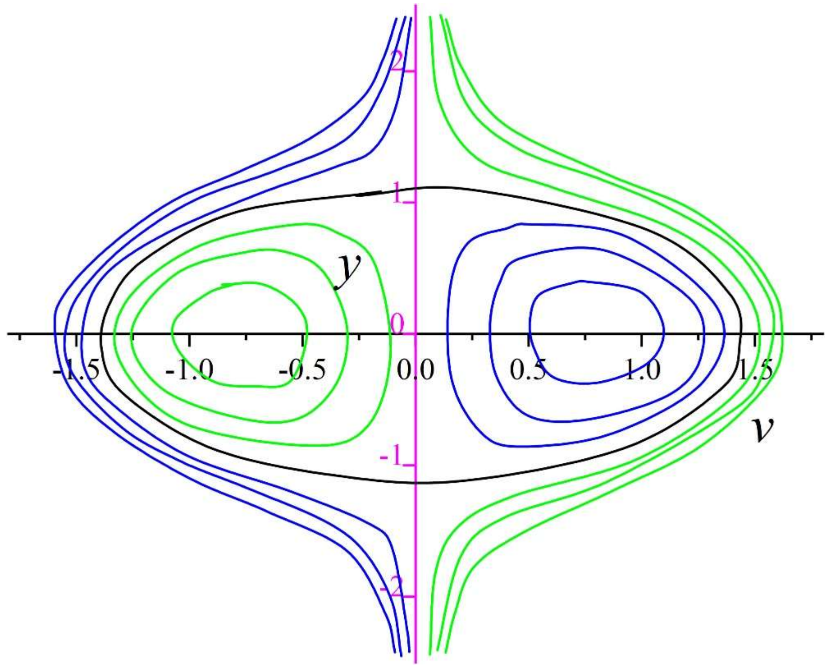

(a) $g>0,\rho>0$

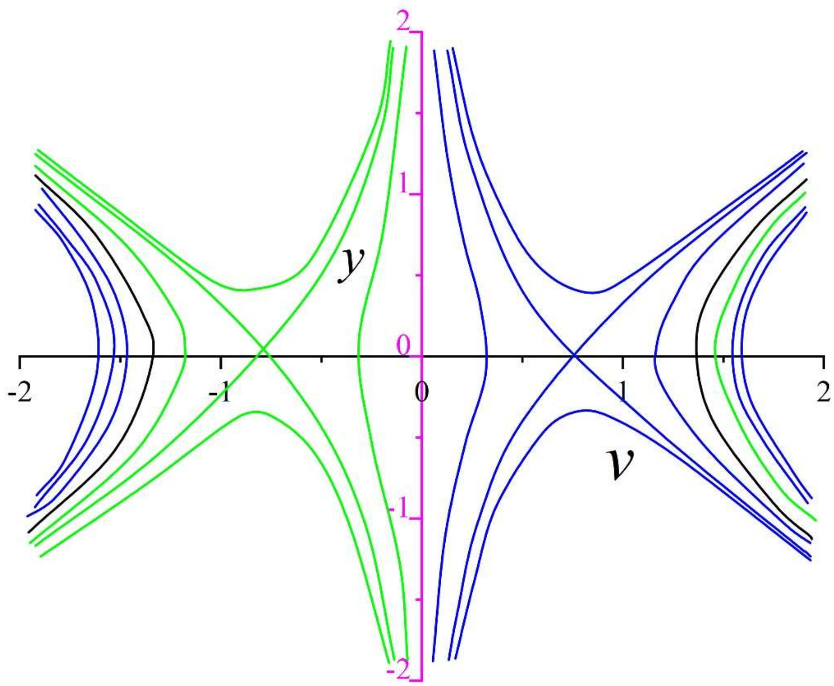

(b) $g>0,\rho<0$

Fig. 2. The plane power system at g>0

3) $g<0$

When $g<0$, $\rho>0$, neither $A_{1,2}(\pm\sqrt{\frac{g}{3}},0)$ nor $B_{1,2}\left(0,\pm\sqrt{\frac{g}{\rho}}\right)$ exists. When $g<0$ and $\rho<0$, only $B_{1,2}\left(0,\pm\sqrt{\dfrac{g}{\rho}}\right)$ exists and is a saddle point. Based on this information, the phase diagram of the planar dynamical system is drawn using Maple software. When $g<0$, the phase diagram of the planar dynamical system is shown in Fig. 3.

Corresponding to the black orbit in Fig. 3(a), substituting $h=h_{B_{1,2}}=0$, Eq. (83) is also derived. Thus, integrating both sides of (83) again under the above parametric conditions yields:

$$
\begin{aligned}
v_7 &= \sqrt{-g}\sinh\left(\frac{x}{\sqrt{-\rho}}+C_7\right)\\
v_8 &= -\sqrt{-g}\sinh\left(\frac{x}{\sqrt{-\rho}}+C_8\right)
\end{aligned}
\tag{92}
$$

where C_7, C_8 are constants. Substituting v_7, v_8 back into the first equation in the planar dynamical system, similar to the calculations in equations (75) and (76), the parametric condition $\beta=\rho$ is also obtained.

Thus, two exact solutions of the KdV-mKdV equations are obtained by substituting v_7, v_8, respectively, when $\beta=\rho$:

$$
u_7 = \sqrt{-g}\sinh\left(\frac{x}{\sqrt{-\rho}}+C_7\right)E_\alpha\left(\lambda t^\alpha\right) \tag{93}
$$

$$
u_s = -\sqrt{-g}\sinh\left(\frac{x}{\sqrt{-\rho}}+C_s\right)E_a\left(\lambda t^\alpha\right) \tag{94}
$$

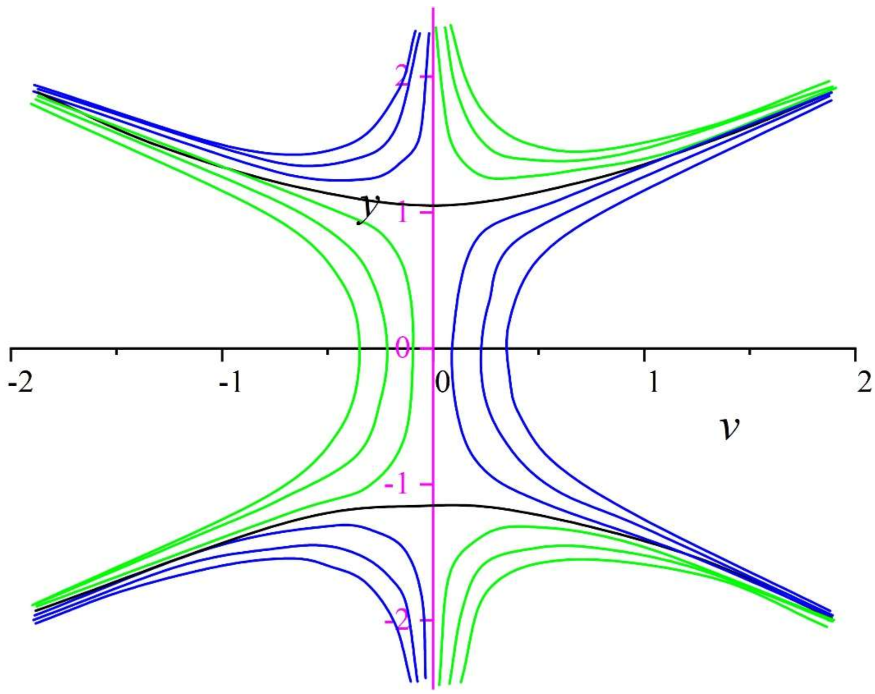

(a) $g<0,\rho<0$

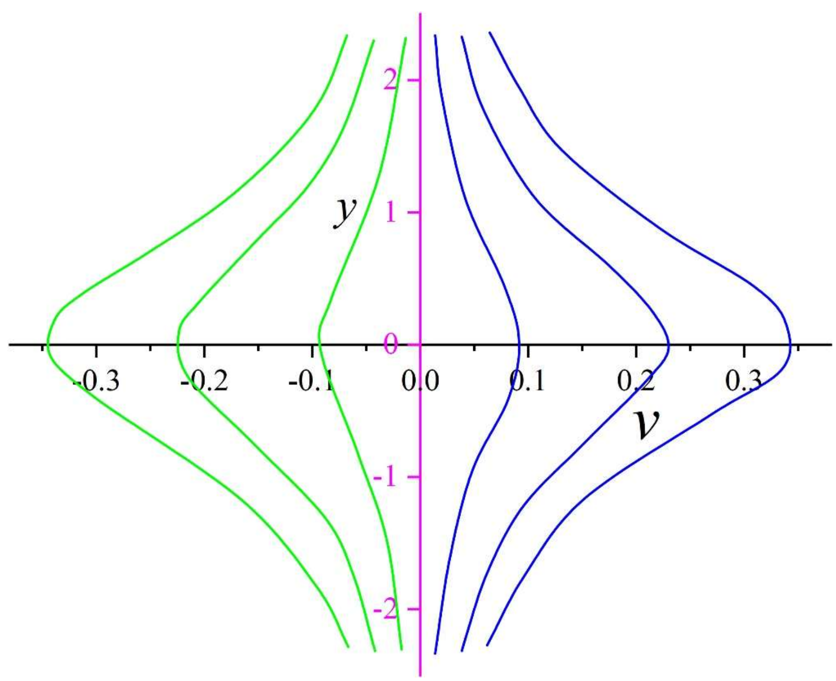

(b) $g<0,\rho>0$

Fig. 3. The plane power system at g<0

4.2. Example 2

In this section, the above analysis will be demonstrated through numerical simulations. When $n=1$ or $n=2$, the equations are solved as initial value problems. The initial condition in the simulation is (0,0,0.1). For closed orbits, the initial condition is a point in a sufficiently small domain of the center. 1) In this paper, Mathematic software is used for simulation and only the case of $z>0$ is considered and the results obtained are shown in Fig. 4. Figure 4 shows the results simulated when $n=1$, ε is sufficiently small. In the figure $n=1$, $\varepsilon=0.00001$, $b=0.03$, $q=0.05$, $s=1$, the projection of the co-located orbitals in three dimensions in the uv plane and the uz diagram. The results show that there exists a homing orbit connecting the zero equilibrium point of the planar dynamical system, which corresponds to a bell-shaped isolated wave.

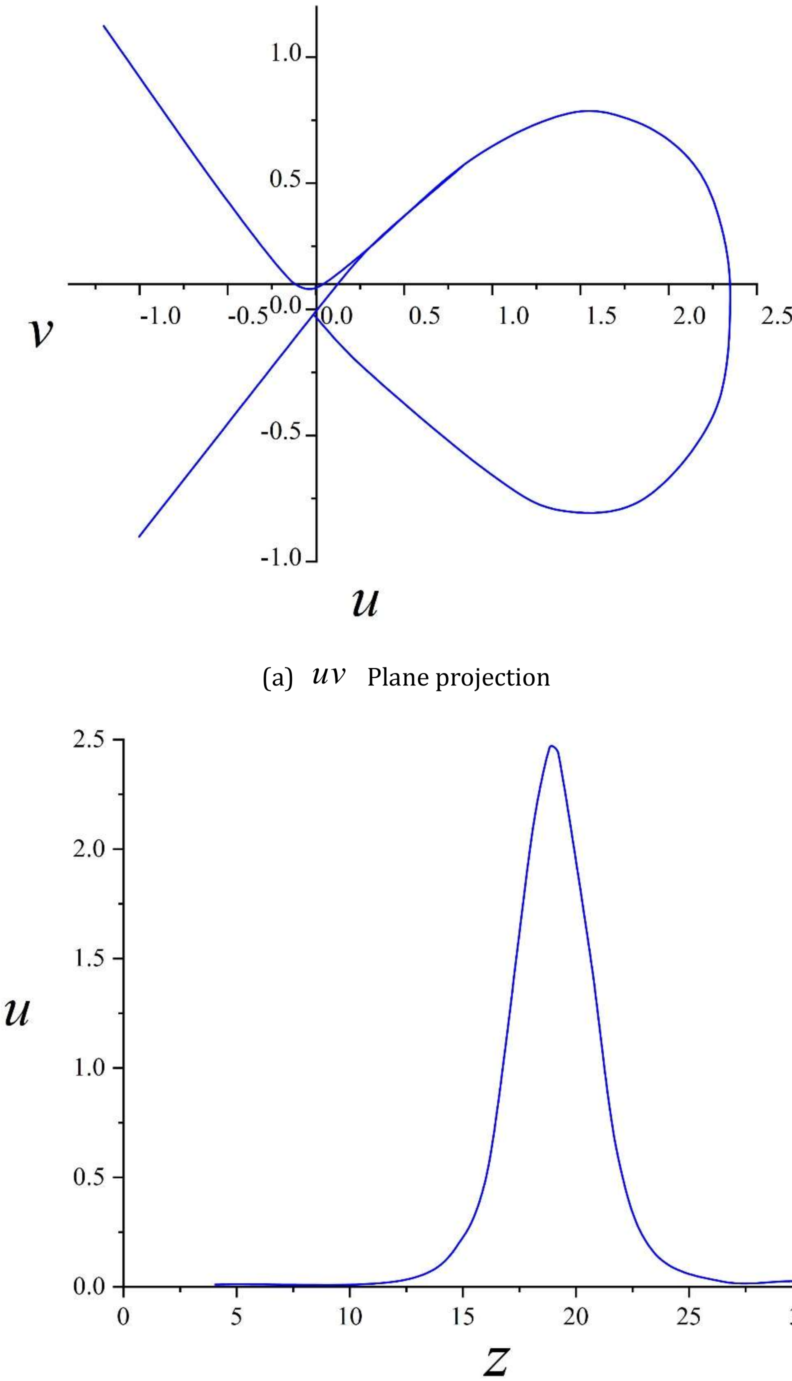

Fig. 4. The plane projection of the same night orbit of the three-dimensional space

2) When $\varepsilon=0.01$, the projection and uz diagram of the co-located orbits in the uv plane in three dimensions are shown in Fig. 5. The other parameter values are $n=1$, $b=0.03$, $q=0.05$, and $s=1$, which are the same as in the above figure. It shows the results simulated when $n=1$, ε is relatively large. The results show that the same-home orbit breaks and the corresponding wave is oscillating.

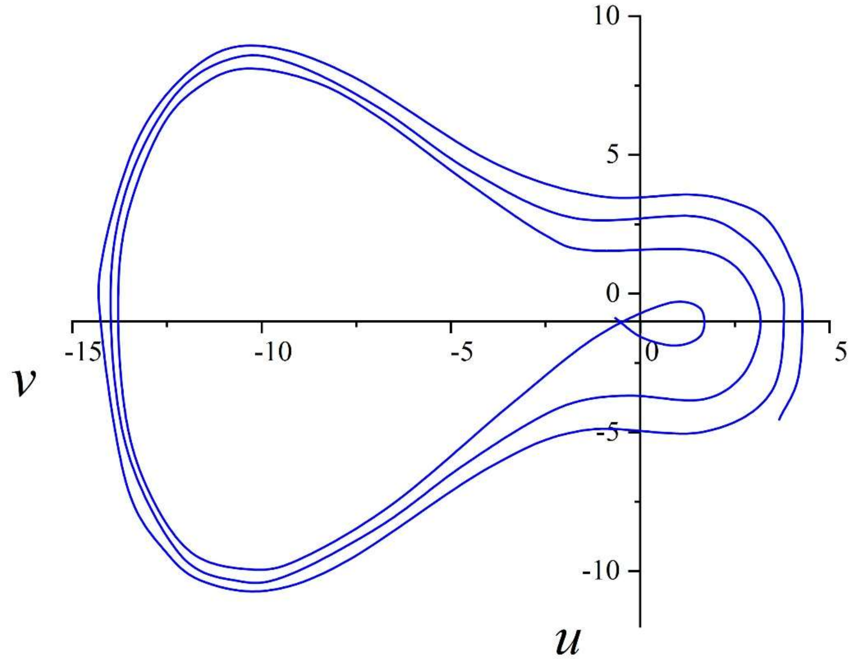

(a) uv Plane projection

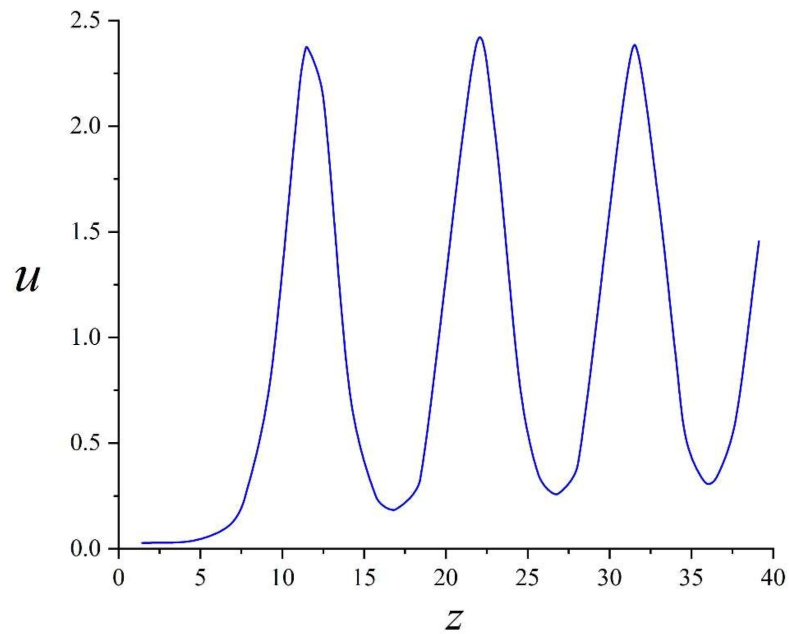

(b) uz

Fig. 5. The homology of three dimensional space

3) When $n=2$, the projection and uz diagram of the co-located orbits in the uv plane in three dimensions is shown in Fig. 6. The figure shows the results simulated when $n=2$, ε is sufficiently small, $\varepsilon=0.00001$, $b=0.03$, $q=0.05$, $s=1$. The results indicate the existence of two homogeneous orbits connecting the zero equilibrium point in the planar dynamical system, and the corresponding waves are a combination of bell-type isolated waves and anti-bell-type isolated waves.

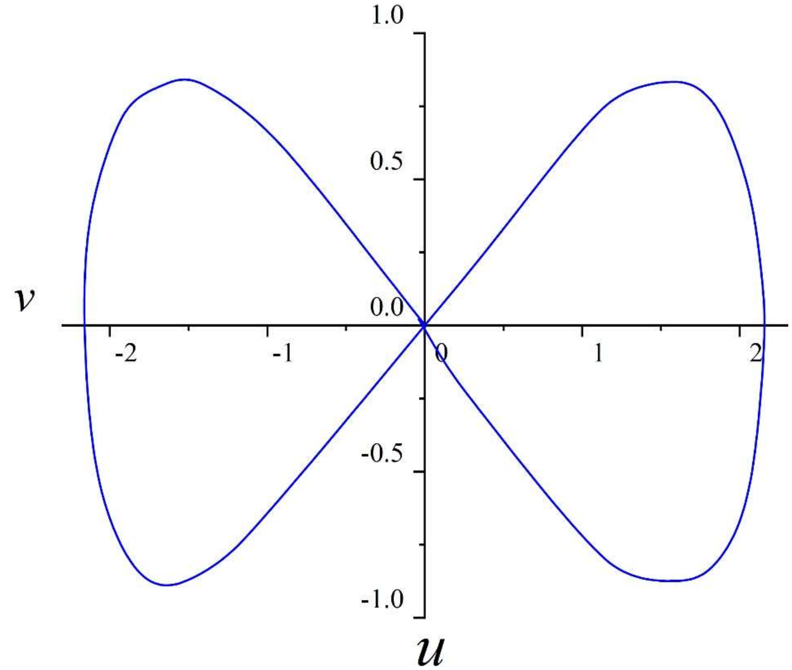

(a) uv Plane projection

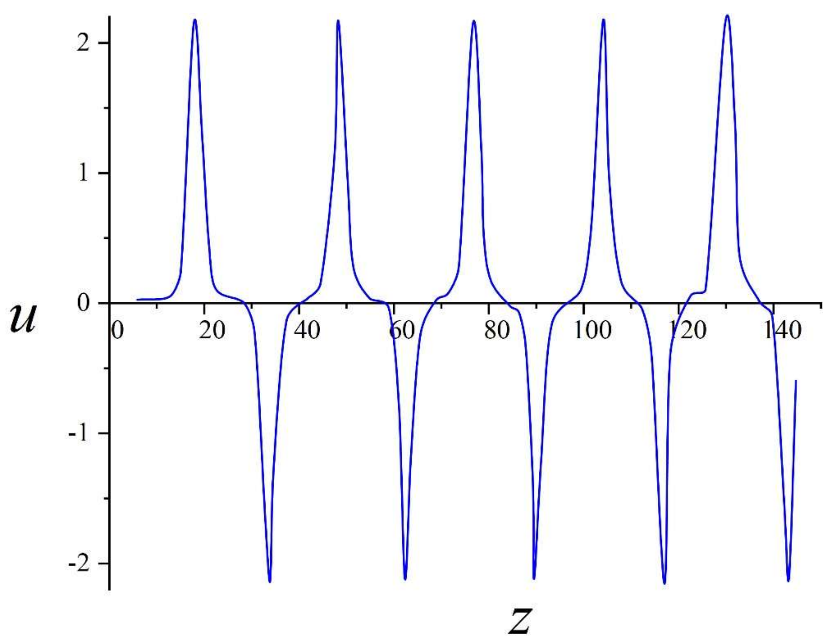

(b) uz

Fig. 6. When the n= 2, three-dimensional space is projected in the same floor

4) When $\varepsilon = 0.1$, the projection of the co-located orbit in the uv plane in three dimensions and the uz diagram are shown in Fig. 7. The parameter values are $n = 2$, $b = 0.03$, $q = 0.05$, and $s = 1$. The figure shows the results simulated when $n = 2$, ε is relatively large. The results show that the same-home orbit breaks and the corresponding wave is oscillating.

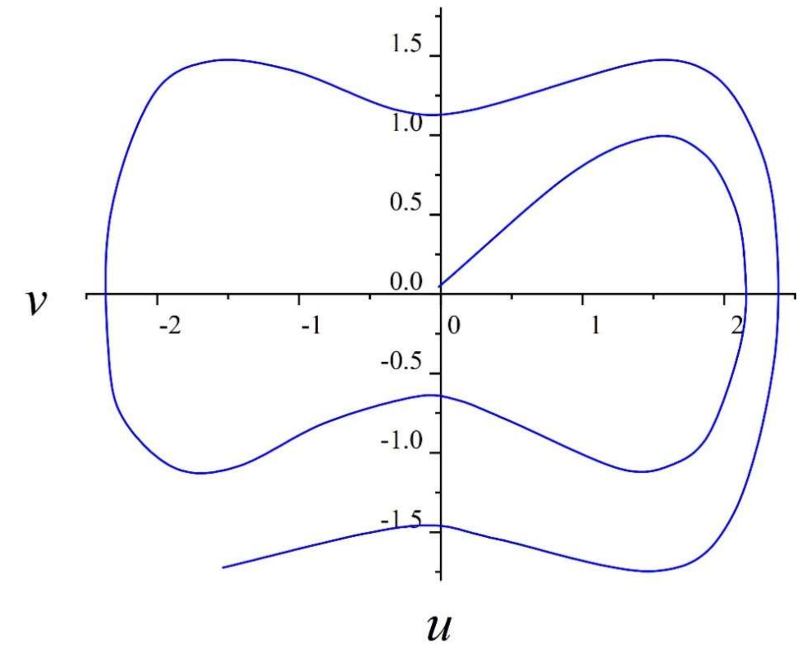

(a) uv Plane projection

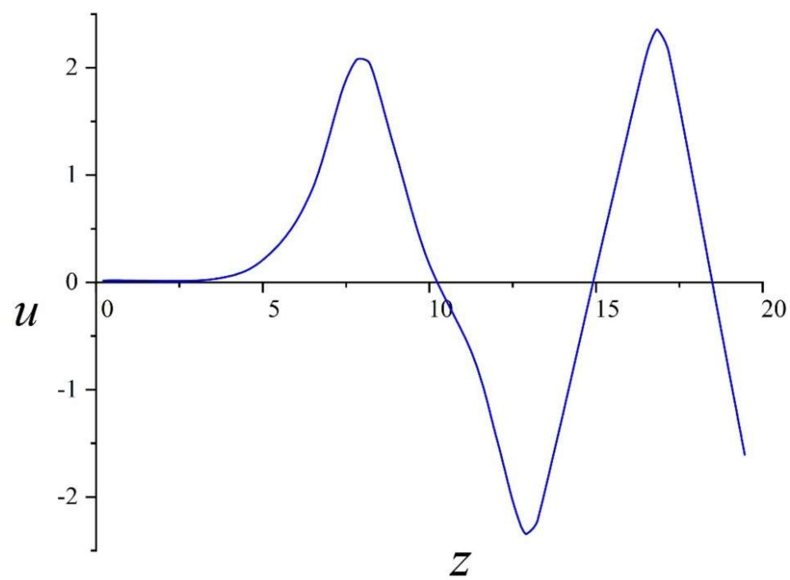

(b) uz

Fig. 7. When the $\varepsilon = 0.1$, three-dimensional space is projected in the same floor

5) The projection and uz diagrams of one heterodyne orbit and two heterodyne orbits in the uv plane in three dimensions are shown in Fig. 8, where $n=1$, $p=-0.3$, $b=1.5$, $q=2$, $\varepsilon=0.00001$, $s=1$. The results are shown for $n=1$, $p=-0.2$, ε simulated at full hours. The results indicate the existence of two heterodyne orbits connecting the zero equilibrium points (0,0,0) and (6,0,0) in the planar dynamical system. One corresponds to a kink-type isolated wave and the other to an anti-twist-type isolated wave.

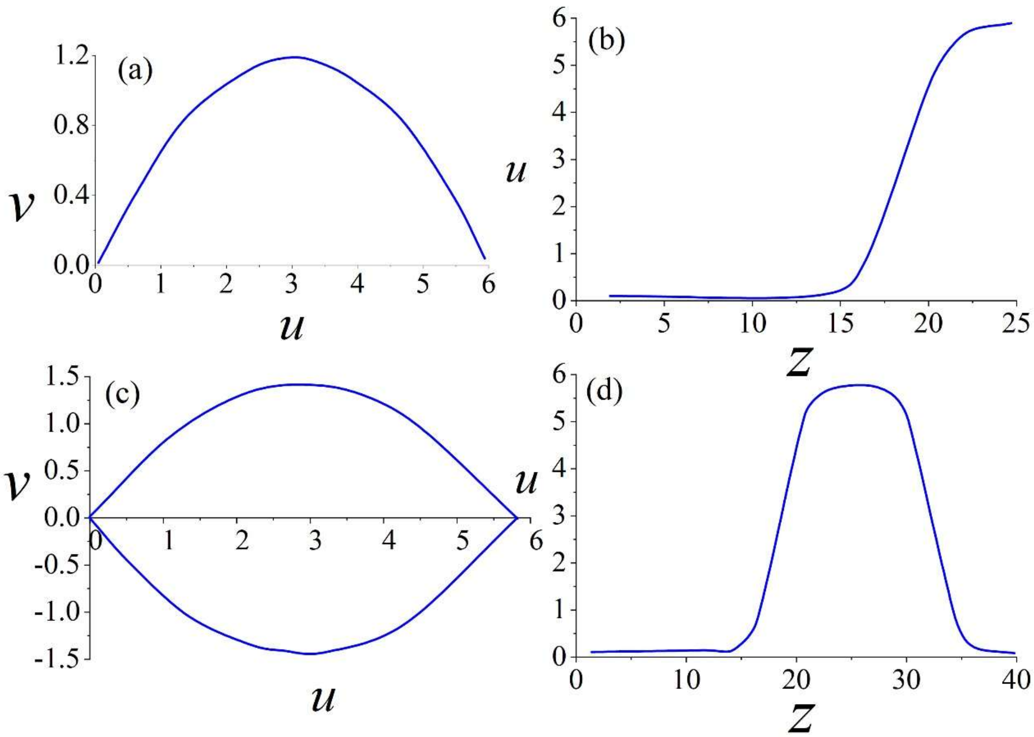

Fig. 8. The screen projection distribution of the isotopic orbit in 3D space

6) When $\varepsilon = 0.1$, the projection and uz diagram of the heterohomogeneous orbits in the uv plane in three-dimensional space are shown in Fig. 9. Fig. 9 shows the simulated results for the simulated data of the above figure when only ε is changed and ε is relatively large. The other parameters are $n=1$, $p=-0.3$, $b=1.5$, $q=2$, $\varepsilon = 0.00001$, and $s=1$.

The results show that when ε is relatively large, the heterodyne orbit becomes connected to the equilibrium points (0,0,0) and (3,0,0), the corresponding wave is oscillating, and u is finally stabilized at the value of 5. A phenomenon can be seen in the fact that the planar dynamical system has three equilibrium points (0,0,0), (6,0,0) and (3,0,0). ε When sufficiently small, the heterohomogeneous orbits are connecting (0,0,0) and (6,0,0). There are two heterohomogeneous orbitals, corresponding to kink-type and anti-twist-type isolated waves. When ε is larger, the heterohoming orbits become connected (0,0,0) and (3,0,0). There is only one heterohomogeneous orbit and it corresponds to an oscillating wave, but the wave stabilizes at a fixed value.

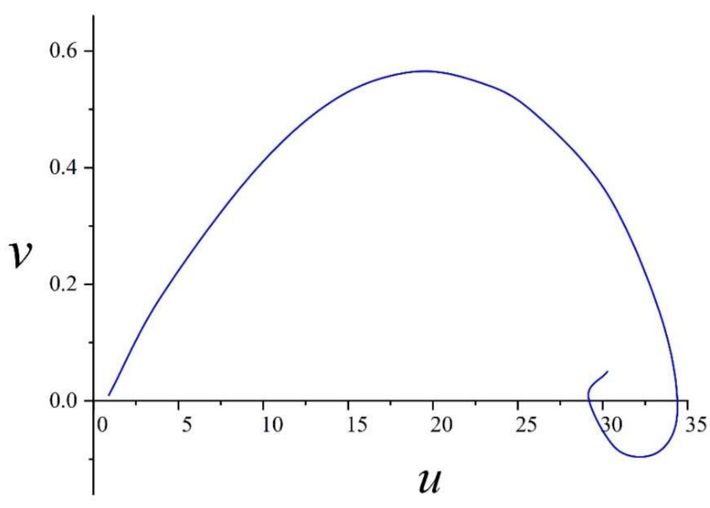

(a) uv Plane projection

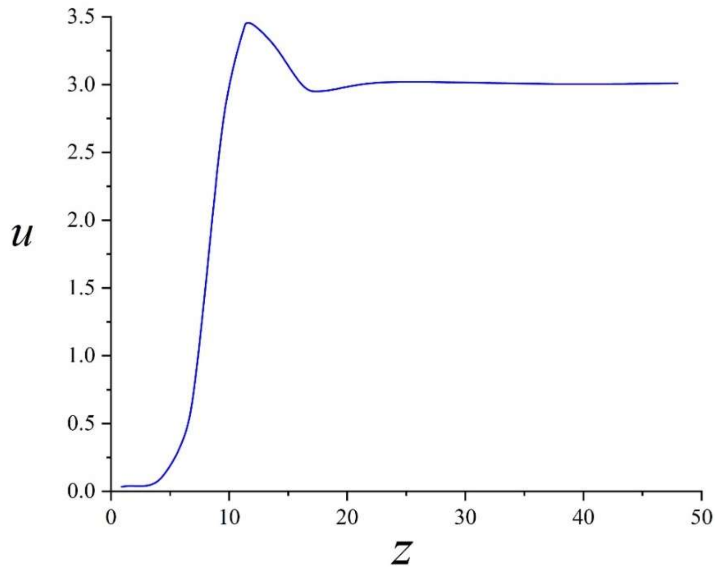

(b) uz

Fig. 9. When $\varepsilon = 0.1$, the flat projection of the isodromic orbit in 3D space

4.3. Example 3

In this section, the following model problems with exact solutions will be selected for numerical tests to verify the stability and accuracy of the format and to analyze the alternating difference method for the KdV-mKdV equations.

Example: take $\beta=5$, $\varepsilon=1$, $p=2$, $L_1=-40$, $L_2=40$, respectively, for the problems (1) to (3), and take the initial conditions of the equations as:

$$u(x,0)=\sqrt{c}\,\mathrm{sech}(\sqrt{c}x+d) \tag{95}$$

At this point the problem has an isolated wave solution:

$$u(x,t)=\sqrt{c}\,\mathrm{sech}(\sqrt{c}(x-ct)+d) \tag{96}$$

Where d denotes the initial crest position of the isolated wave, $\sqrt{c}$ denotes the crest height of the isolator, $\sqrt{c}$ in the positive cut function denotes the abrupt steepness of the isolator, and c denotes the speed of the isolator, where $d=0$ is chosen.

Assuming that $u_i^n=u(x_i,t_n)$ and v_i^n denote the exact and numerical solutions of the problem, respectively, the L_2 modes and the L_∞ modes of their errors are computed in the following form:

$$\begin{aligned} E_{\infty,\Delta x} &= \max_i\left(e^n_{\Delta x,\Delta t}(i)\right)=\max_i\left|u_i^n-v_i^n\right| \\ E_{2,\Delta x} &= \left\|e^n_{\Delta x,\Delta t}\right\|_2=\max_i\sum_i\sqrt{\left|u_i^n-v_i^n\right|^2\Delta x} \end{aligned} \tag{97}$$

Where Δx, Δt are the spatial step and time step respectively.

Take the time step Δt = 10^{-6}, and the spatial step Δx = 90/300, 90/400, 90/500, 90/600 respectively for comparison.

When c =0.6, T =0.01, n =10,000 time steps, the errors at different grid ratios show that the alternating grouping algorithm decreases as the spatial step size decreases, the L_2 modes and the L_∞ modes decrease accordingly, and the order of convergence is approximately $O(h^2)$, these values experimental results are consistent with the theoretical analysis.

The errors of the alternating grouping algorithm at M of 400, 500, 600, 700, c=0.6, n=10000 time steps are given below, respectively. Comparing the analytical results in the table, it can be obtained that a set of asymmetric difference formats is constructed on the basis of the idea of alternating grouping and a new class of alternating grouping algorithms for solving the KdV-mKdV equations is designed. Theoretical analysis shows that the algorithm is unconditionally stable and intrinsically parallel. Numerical results show that the alternating grouping algorithm proposed in this paper is unconditionally stable and can be intrinsically parallel.

The errors when c=0.6, M=400, T=0.01, n=10000 time steps are shown in Table 1. The specific error values for n taking values from 2000 to 10000 time steps are recorded in the table respectively. When c=0.6, M=400, T=0.01, n=10000 time steps, the error range is [1.0299e-0.15,1.8930e-0.15].

Table 1. The error of the M=400 time, the 10,000 time step

steps	x			
	-30	-10	10	30
2000	3.3263e-0.15	3.2516e-0.15	1.8963e-0.15	2.8546e-0.15
4000	6.8563e-0.15	4.1253e-0.15	3.5261e-0.15	5.5291e-0.15
6000	9.0425e-0.15	6.3318e-0.15	5.9844e-0.15	8.3326e-0.15
8000	1.3263e-0.15	8.2659e-0.15	7.4270e-0.15	1.1245e-0.15
10000	1.8930e-0.15	1.0537e-0.15	1.0299e-0.15	1.3596e-0.15

The errors when c=0.6, M=500, T=0.01, and n=10000 time steps are shown in Table 2. The data in the table shows that the minimum error is 2.4535e-0.15 when n=10000 time steps.

Table 2. The error of the M=500 time, the 10,000 time step

steps	x			
	-30	-10	10	30
2000	1.0251e-0.15	4.9686e-0.15	4.8969e-0.15	9.0254e-0.15
4000	2.0854e-0.15	9.7854e-0.15	9.9243e-0.15	1.0899e-0.15
6000	3.1217e-0.15	1.5208e-0.15	1.5207e-0.15	2.9813e-0.15
8000	4.2398e-0.15	1.9637e-0.15	1.9689e-0.15	3.7254e-0.15
10000	5.0123e-0.15	2.5251e-0.15	2.4535e-0.15	4.6587e-0.15

The errors when c=0.6, M=600, T=0.01, and n=10000 time steps are shown in Table 3. Comparison of the data in the table shows that the maximum error is 6.9609e-0.15.

Table 3. The error of the M=600 time, the 10,000 time step

steps	x			
	-30	-10	10	30
2000	4.2635e-0.15	1.2142e-0.15	1.4574e-0.15	3.8756e-0.15
4000	8.5291e-0.15	2.4535e-0.15	2.8965e-0.15	7.7554e-0.15
6000	1.3311e-0.15	3.8961e-0.15	4.2634e-0.15	1.1245e-0.15
8000	1.5986e-0.15	4.9568e-0.15	5.5696e-0.15	1.5263e-0.15
10000	2.0351e-0.15	6.2131e-0.15	6.9609e-0.15	1.8969e-0.15

The errors when c=0.6, M=700, T=0.01, and n=10000 time steps are shown in Table 4. The error is maximized when x takes the value of 30 and n=10000 time steps.

Table 4. The error of the M=700 time, the 10,000 time step

steps	x			
	-30	-10	10	30
2000	2.3261e-0.15	1.2543e-0.15	3.2445e-0.15	1.8969e-0.15
4000	4.1521e-0.15	2.6597e-0.15	6.3211e-0.15	3.7548e-0.15
6000	6.2527e-0.15	4.4573e-0.15	9.0214e-0.15	5.5362e-0.15
8000	8.3259e-0.15	6.6594e-0.15	1.1433e-0.15	7.4757e-0.15
10000	1.3352e-0.15	8.8968e-0.15	1.5789e-0.15	9.3268e-0.15

5. Conclusion

In this paper, the general form of the hybrid KdV-mKdV equation, i.e., $u_t + \alpha u u_x + \beta u^2 u_x + \gamma u_{xxx} = 0$, is presented, where Eq. describes the amplitude of the associated wave. The N soliton solution of the hybrid KdV-mKdV equation and its determinant form are analyzed, and the difference function is constructed to solve the KdV-mKdV equation.

The solution of the KdV-mKdV equation and its dynamical properties are discussed by the semi-fixed separation of variables method combined with the phase diagram analysis of the dynamical system in Example 1. Some exact solutions are obtained under the compatibility condition $\beta = \rho$. It is shown that none of these solutions contain soliton solutions or periodic solutions. And all the solutions decay in amplitude as time increases.

The influence of the value of n on the existence of soliton solutions of the KdV-mKdV equation is considered in Example 2. A step-by-step demonstration of the existence of transverse homodyne orbits, and hence the existence of an isolated wave solution to the KdV-mKdV equation, is shown.

Example 3 applies the alternating grouping algorithm constructed in the paper to solve the KdV-mKdV equation, demonstrating the stability of the proposed alternating grouping algorithm as well as the fact that it can be intrinsically parallelized.

References

[1] Kasman, A. (2018). A brief history of solitons and the KdV equation. Current Science, 115(8), 1486-1496.

[2] Oblak, B., & Kozyreff, G. (2020). Berry phases in the reconstructed KdV equation. Chaos: An Interdisciplinary Journal of Nonlinear Science, 30(11).

[3] Vivas-Cortez, M., Akram, G., Sadaf, M., Arshed, S., Rehan, K., & Farooq, K. (2023). Traveling wave behavior of new (2+ 1)-dimensional combined KdV–mKdV equation. Results in Physics, 45, 106244.

[4] Ali, N. H., Mohammed, S. A., & Manafian, J. (2024). Study on the simplified MCH equation and the combined KdV–mKdV equations with solitary wave solutions. Partial Differential Equations in Applied Mathematics, 9, 100599.

[5] Yuan, R. R., Shi, Y., Zhao, S. L., & Zhao, J. X. (2023). The combined KdV-mKdV equation: Bilinear approach and rational solutions with free multi-parameters. Results in Physics, 55, 107188.

[6] Ishimura, N. (2020). Research on Nonlinear Partial Differential Equations in Mathematical Finance. Impact, 2020(8), 48-50.

[7] Dong, Y., Liu, T., Li, Z., & Qiao, P. (2023). DeepFEM: A novel element-based deep learning approach for solving nonlinear partial differential equations in computational solid mechanics. Journal of Engineering Mechanics, 149(2), 04022102.

[8] Singh, S., & Saha Ray, S. (2017). Exact solutions for the Wick-type stochastic Kersten-Krasil'shchik coupled KdV-mKdV equations. The European Physical Journal Plus, 132, 1-12.

[9] Farooq, A., Khan, M. I., & Ma, W. X. (2024). Exact solutions for the improved mKdv equation with

conformable derivative by using the Jacobi elliptic function expansion method. Optical and Quantum Electronics, 56(4), 542.

[10] Zhang, Y., Dong, H., Sun, J., Wang, Z., Fang, Y., & Kong, Y. (2021). The New Simulation of Quasiperiodic Wave, Periodic Wave, and Soliton Solutions of the KdV - mKdV Equation via a Deep Learning Method. Computational Intelligence and Neuroscience, 2021(1), 8548482.

[11] Hussain, E., Mahmood, I., Shah, S. A. A., Khatoon, M., Az-Zo'bi, E. A., & Ragab, A. E. (2024). The study of coherent structures of combined KdV-mKdV equation through integration schemes and stability analysis. Optical and Quantum Electronics, 56(5), 723.

[12] Wang, K. J. (2022). Bäcklund transformation and diverse exact explicit solutions of the fractal combined KdV–mKdV equation. Fractals, 30(09), 2250189.

[13] Kaya, D., Gülbahar, S., Yokuş, A., & Gülbahar, M. (2018). Solutions of the fractional combined KdV–mKdV equation with collocation method using radial basis function and their geometrical obstructions. Advances in Difference Equations, 2018(1), 77.

[14] Raza Rizvi, S. T., Ali, K., Sardar, A., Younis, M., & Bekir, A. (2017). Symbolic computation and abundant travelling wave solutions to KdV–mKdV equation. Pramana, 88, 1-6.

[15] Ullah, M. A., Rehan, K., Perveen, Z., Sadaf, M., & Akram, G. (2024). Soliton dynamics of the KdV–mKdV equation using three distinct exact methods in nonlinear phenomena. Nonlinear Engineering, 13(1), 20220318.

[16] Ahmad Aliyari Boroujeni,Reza Pourgholi & Seyed Hashem Tabasi. (2025). Numerical solutions of KDV and mKDV equations: Using sequence and multi-core parallelization implementation. Journal of Computational and Applied Mathematics,454,116184-116184.

[17] Zheng Xiaoxiao,Xin Jie & Gu Yongyi. (2020). Orbital stability of solitary waves to the coupled compound KdV and MKdV equations with two components. AIMS Mathematics,5(4),3298-3320.

[18] Xiaoxiao Zheng & Hui Wu. (2020). Orbital stability of periodic traveling wave solutions to the coupled compound KdV and MKdV equations with two components. Mathematical Foundations of Computing,3(1),11-24.

[19] Zhi Guo Liu,Muhua Liu & Jinliang Zhang. (2024). Sech 2 -type solitary waves and the stability analysis for the KdV-mKdV equation.. Scientific reports,14(1),16315.

[20] Chu Han Shang & Huai An Yi. (2024). SOLUTIONS OF THE KDV-MKDV EQUATIONS ARISING IN NON-LINEAR ELASTIC RODS UNDER FRACTAL DIMENSION. Thermal Science,28(3A),2125 - 2133.